18th Australasian Fluid Mechanics Conference
Launceston, Australia
3-7 December 2012

Reynolds-Averaged Navier-Stokes Computation of Transonic Projectiles in Ground Effect

Kate Carriage[1], John Young[1], Harald Kleine[1] and Koju Hiraki[2]

[1]School of Engineering and Information Technology
University of New South Wales, Canberra, 2600, Australia

[2]Department of Mechanical and Control Engineering
Kyushu Institute of Technology, Kitakyushu, Fukuoka 804-8550, Japan

Abstract

As a transonic projectile passes near a solid object, its surrounding flow field changes quite considerably: the bow shock naturally adopts a strong solution and pushes forward from its free-flight position, and the projectile's wake is pulled down towards the object. These phenomena were first captured separately by schlieren imaging techniques during live fire and wind tunnel testing. A subsequent computational study, performed in Fluent at a free stream pressure of 72 kPa and for a projectile Mach number of 1.1, demonstrated that the presence of the wall introduces aerodynamic forces whose magnitude and direction can become significant for the subsequent projectile trajectory. The lift force was found to be up to ten percent of the projectile's drag, and may be either positive or negative depending on the proximity to the ground. Similarly, the coefficient of moment may be either positive or negative with a neutral point that does not coincide with the point of zero lift. The results are pertinent to many fields including aircraft weapons release and low level operations, wing-in-ground effect vehicles, and vehicles designed to challenge the land speed record.

Nomenclature

C_D	=	coefficient of drag based on frontal area
C_L	=	coefficient of lift based on planform area (normal to the ground plane, away from the ground +ve)
C_M	=	coefficient of moment based on planform area and projectile length (nose down +ve)
d	=	diameter of projectile [m]
h	=	distance from ground plane to outer margin of projectile [m]
l	=	length of projectile [m]
M	=	Mach number
s	=	shock standoff distance from projectile nose [m]

Introduction

The mechanical behaviour of projectiles in flight has attracted wide-spread attention since the advent of the firearm. Investigation into such characteristics, known as external ballistics, has been made much easier with advances in high-speed flow visualisation and numerical simulation techniques. The existing focus on stability and long range accuracy has recently been extended to ground effect studies which investigate the aerodynamic changes that occur when flying close to an immovable boundary at supersonic speeds [1, 3, 6].

In the subsonic regime, the extra lift or down force from ground effect is exploited in the design of fast watercraft [2] and in Formula 1 and other forms of racing. Supersonic and transonic ground effect has understandably received much less attention, although similar aerodynamic effects are observed in military aircraft weapon release [4], high-speed aircraft entering very low level flight, and even land speed records [5]. Transonic and supersonic projectiles are often fired in close proximity to walls in urban conflict environments. A previous computational and experimental study of a supersonic ($M = 2.4$) projectile in ground effect found minimal variation of lift, drag and moment coefficient with ground separation ratio h/d, while the oblique shock from the projectile nose reflected back into the far or near near wake [1]. At about $h/d = 1.0$ the bow shock reflection started to impinge onto the projectile itself and with further reduction in h/d, lift increased rapidly, drag first slightly decreased then increased rapidly, and the pitching moment followed a similar trend to the drag. Experimental investigation of a transonic ($M = 1.1$) projectile found that in contrast to the supersonic projectile, the presence of the ground led to a growth of the subsonic zone behind the bow shock, which in turn changed shape and position of the shock, which over a range of clearances was seen to bend forward or to straighten and move away from the projectile, in each case avoiding the establishment of a reflected shock off the ground [3]. Hence, there is solid reason to extend our understanding of the aerodynamic properties of ground effect, particularly in the understudied area of transonic flight. This work extends the experimental study [3] with a computational fluid dynamics (CFD) investigation across a wider range of h/d values.

Numerical Method

Simulations were designed to replicate the flow conditions and projectile geometry and scale used in the experimental wind tunnel tests [3]. This was a 7.5:1 scale model of a Nosler 50 grain S.H.O.T. projectile.

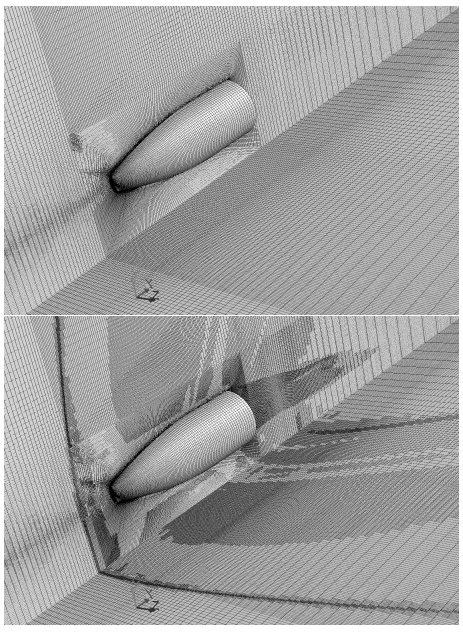

Figure 1: Baseline (1.19 million cells, upper frame) and refined (4.59 million cells, lower frame) meshes for the $h/d = 0.5$ case.

Rifling striations and stabilising spin were neglected in the model, based on very close similarity between spinning and non-spinning forces in previous work [1] and the low spin rate of this projectile. The flow field was modeled in three dimensions, with a symmetry plane through the long axis of the projectile, and a moving ground plane underneath the projectile, as shown in figure 1. The free stream pressure was 72000 Pa, with Mach number $M = 1.1$. The ground plane moved at $M = 1.1$ in relation to the projectile. For the free flight (no ground effect) case, a second symmetry plane, again through the long axis of the projectile, was used instead of the ground plane (thus one quarter of the domain was simulated). Distances to boundaries were: inlet 1.0, outlet 12.0, and far field 12.0 projectile lengths respectively.

Simulations were performed with the commercial 64-bit finite volume code Fluent 13.0, using an implicit density-based solver with second-order upwind spatial discretisation. Flow was assumed fully turbulent at the inlet, with intensity 0.1% and turbulent viscosity ratio 0.1, to simulate the projectile flying into quiescent air. $k-\omega$ SST and Spalart Allmaras turbulence models were compared, with negligible differences in flow field or aerodynamic forces, however the $k-\omega$ SST model showed more rapid convergence and was used throughout. Convergence was considered achieved when the change in total pressure on the projectile was less than 0.1% over 500 successive iterations. Conservation of mass was maintained, with mass flux imbalance being less than 0.001% of inlet flux in all cases. The turbulent y^+ values at the wall of the projectile were everywhere less than 3.0. The bow shock from the projectile was observed to reflect off the far field boundary back into the domain, approximately $8.0l$ aft of the projectile, well beyond the region of interest. Mesh refinement was conducted in regions of high pressure gradient in each case, to better capture shocks and expansions as shown in figure 1. For the $h/d = 0.5$ case this increased the mesh cell count from 1.19 million (baseline) to 4.59 million (refined), values typical for the other h/d cases considered. Lift, drag and pitching moment coefficients varied less than 2.5% from baseline to refined meshes.

Results and Discussion

Shock Behaviour

The flow field on the symmetry plane is shown in figure 2, in the form of contours of velocity magnitude, for a range of h/d values. A number of features are immediately apparent in this visualisation. The first is that at this Mach number ($M = 1.1$) the bow shock from the nose of the projectile does not reflect off the ground plane, as was observed in the earlier higher speed ($M = 2.4$) study [1]. Instead, the bow shock curves to meet the ground plane at a right angle (very apparent in the $h/d = 2.0$ case in the bottom frame of figure 2). This is in contrast to the recompression shocks downstream of the projectile base, which reflect obliquely off the ground. The radius of curvature of the projectile nose used here is such that the leading shock wave is a detached bow shock for all Mach numbers greater than 1.0. In the free-flight case, this bow shock is normal to the axis of the projectile and gradually inclines until it develops into a Mach wave in the far field. Thus the detached bow shock exhibits all possible oblique shock solutions at once for the given free stream conditions. The flow past the shock wave will be either subsonic or supersonic depending on whether a strong or weak solution exists, respectively. Figure 3 shows an experimental flow visualisation for approximately $h/d = 1.0$, showing a number of similarities with the CFD case, including deflection of the wake towards the groundplane and near-normal recompression shock interacting with the wake at about $l/d = 0.8$ aft of the projectile base. The experimental results [3] show no bow shock

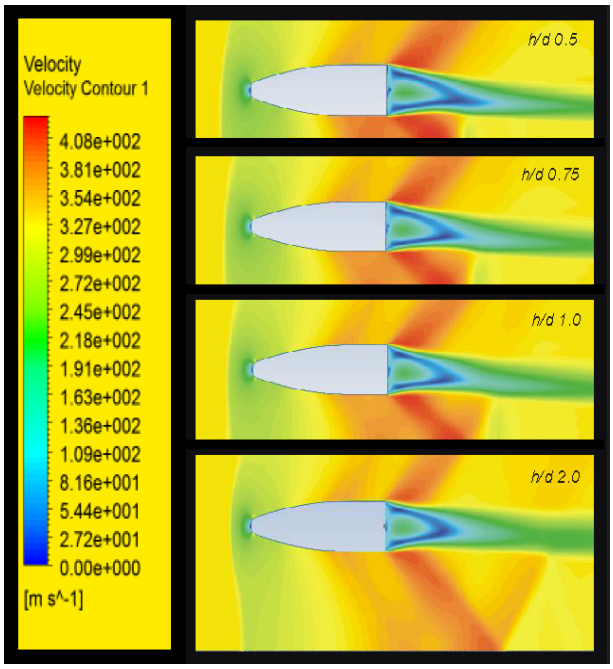

Figure 2: Flow field behaviour as a function of ground separation distance h/d.

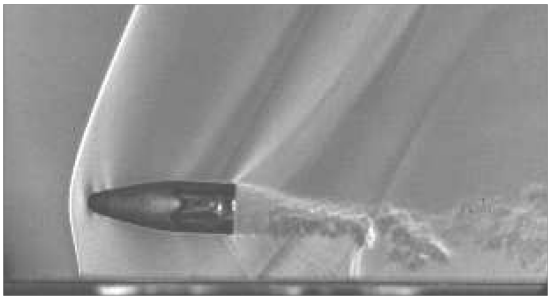

Figure 3: Experimental live-fire schlieren image of the flow field for approximately $h/d = 1.0$ from [3].

reflection at $h/d = 0.5$, but for $h/d = 1.6$ there is no straightening of the bow shock as it nears the ground, and reflection of the oblique wave as observed in the $M = 2.4$ study. This apparently contradictory behaviour has been explained by preliminary unsteady time-accurate simulations of the projectile passing over a corner which show that as it enters ground effect, the bow shock transitions between an oblique reflecting state to a normal non-reflecting state, which is the asymptotic steady-state behaviour. This process takes some considerable time to complete, such that the projectile is in excess of twelve lengths l downstream of the corner when the shock position becomes stable. Since the photographs in the experimental study were taken when the projectile was less than five lengths l downstream of the corner, it is now apparent that the shock structure in this work is not yet in equilibrium.

Figure 4 shows the subsonic and supersonic regions for the free-flight projectile with the $h/d = 0.5$ image superimposed. The presence of the ground not only influences the flow underneath the projectile, but also affects the bow shock characteristics above the projectile. In ground effect the strong shock solution section extends much farther away from the projectile as indicated by the dotted sonic line encircling the subsonic zone. As the distance between the ground and the projectile increases,

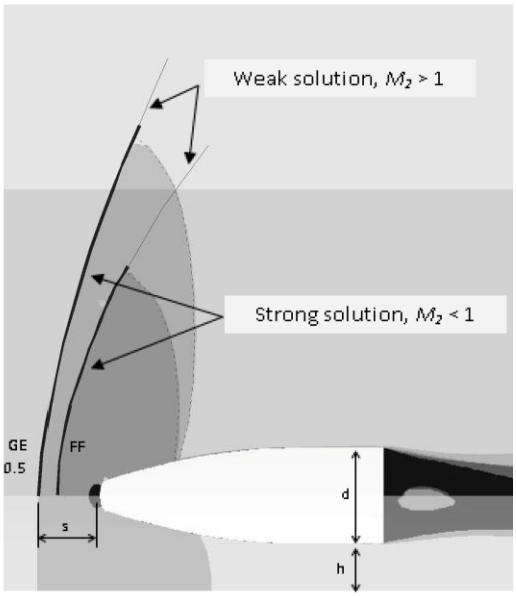

Figure 4: Overlay of free-flight (FF) and $h/d = 0.5$ ground effect (GE) simulations showing the subsonic (shaded regions behind the strong shock solutions) and supersonic zones, and the increased shock standoff distance in the ground effect case.

the subsonic zone shrinks towards the size it has in the free-flight condition. Shock reflections only occur where the flow is locally supersonic. Reflection of the bow shock in the transonic case should, as a first estimate, occur at a distance from the ground where the weak solutions begin on the bow shock. Figure 4 demonstrates this distance to be under 2.25 diameters, however, no shock reflection is evident at equilibrium, even up to a height of 4.5 diameters above the ground. In all cases, the bow shock curves to meet the ground at a right angle, creating a normal shock (and hence a subsonic flow region where the shock meets the ground). This behaviour remains to be fully explored and explained.

Previous studies on supersonic bluff bodies show that the bow shock stand-off distance s is a function of geometry, Mach number and free stream properties [3, 1]. In the case of ground effect, the stand-off distance also varies with the ground separation distance. The bow shock pushes forward of its free-stream position as the projectile transits closer to the ground plane. Figure 5 depicts the strong relationship between the stand-off ratio s/d, and the ground separation ratio h/d. The mesh resolution of the shock in the computational fluid dynamic simulations places the shock within an accuracy of ± 0.03 diameters. The CFD predicted stand-off distances for the bow shock are consistently lower than the wind-tunnel results, even though in both cases the flow has reached full equilibrium (note that the experimental results from the live-fire tests are not included here as in these tests the flow had not yet reached steady state). The larger stand-off distances in the wind tunnel tests is most likely the consequence of a mild blockage effect, which is qualitatively shown by the fact that this discrepancy increases with h/d (i.e. larger sting supports). Additional experimental work with live-fire results taken at much longer trajectory distances downstream of the ground plane corner, coupled with transient simulation, are necessary to fully clarify this effect.

Wake Behaviour

The second prominent feature of the flow fields shown in figure 2 is the behaviour of the wake as a function of ground separation distance h/d. Compared to the free-flight case where the wake is symmetrical, in the ground effect cases the wake is deflected towards the ground plane.The recirculation regions and low-speed flow inside the wake are encapsulated by the shear layer across which there is a substantial velocity gradient. Outside of the wake, the flow speed is of the same order of magnitude as the free stream velocity. Successive Mach waves originate from the region above the narrowest point of the wake, and combine at a distance to form a recompression shock. Geometrical flow constraints underneath the wake force the lower section of the recompression shock to become close to normal at approximately $0.5l$ aft of the projectile for $h/d = 0.5$. As the ground separation distance increases the recompression shock wave interacts with the recirculation zone further downstream. The largest geometrical change in the wake is seen at the closest distance to the ground, where the shock impinges nearest the stagnation point in the wake. Beyond $h/d = 1.0$, the shock wave tends to become more oblique and the wake region becomes relatively symmetrical.

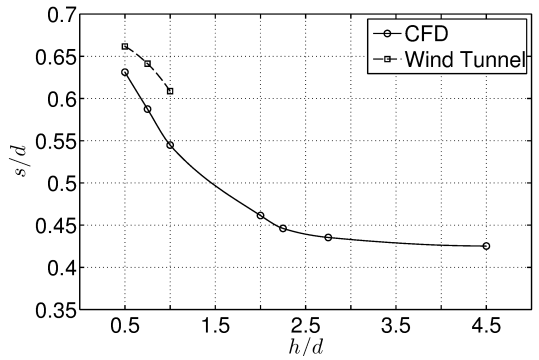

Figure 5: Shock standoff distance s/d as a function of ground separation distance h/d, comparison of simulation and experiment [3].

The recirculating flow aft of the projectile base is seen on the symmetry plane as two low pressure regions. These are symmetric about the projectile axis in the free-flight case. When the projectile enters ground effect the low pressure region closest to the ground plane decreases in extent with respect to the upper region. The two points of lowest pressure in the wake (the centres of the recirculation regions) on the symmetry plane move closer to the projectile's base as the ground separation distance increases from $0.5 < h/d < 2.0$, then move away again for higher h/d. The centre of pressure on the base of the projectile follows a similar trend, moving further above the axis for $0.5 < h/d < 2.0$, then back towards the axis for greater h/d.

Aerodynamic Force Coefficients

The proximity of the projectile to the ground has marked effects on the forces generated and the consequent static stability. Lift, drag and pitching moment were found to be smooth and continuous functions of h/d between the tested ground separation distances. Three distinctly different conditions exist as shown in figure 6 (upper frame). For $0.5 < h/d < 0.85$ the projectile is pulled towards the ground plane (i.e. negative lift) with a nose up (negative) pitching moment. For $0.85 < h/d < 1.5$ the lift force becomes positive so that the projectile is pushed away from the ground, and the pitching moment remains nose up. For $h/d > 1.5$ the lift force increases more slowly but the pitching moment now acts to rotate the nose towards the ground. Based on the tested h/d values, both lift and pitching moment peak somewhere around $h/d = 2.75 - 3.0$, and for higher distances from the ground decrease back towards their free-flight values

of zero. The fact that the lift and pitching moment coefficients do not pass through zero at the same h/d value can be explained by noting that the pitching moment is determined by the magnitudes and lines of action of both the lift and the drag (whereby a low pressure on the projectile base below the centreline axis of the projectile will result in a nose down pitching moment contribution).

As shown in figure 6 (lower frame) the coefficient of drag remains relatively constant for $h/d < 1.25$, and then decreases to approximately the free flight value ($C_D = 0.499$) by $h/d = 4.5$. The overall change in the coefficient of drag is relatively small compared the change in the coefficient of lift, as might be expected given the bluff nature of the projectile geometry. For $h/d = 0.5$, the magnitude of the lift force is approximately 10% of the drag force. The effect of the lift force and pitching moment on projectile stability will be complicated by the stabilising spin imparted upon firing. The pitching moment leads to a Magnus force that may be either destabilising or stabilising depending on the location of the projectile's centre of pressure with respect to its centre of gravity. The lift force will act in the lateral plane due to gyroscopic effects and will tend to turn the bullet left or right depending on the direction of spin. As soon as the projectile responds to the forces and moments through precession, the aerodynamics will change considerably. Thus, the dynamic response of the projectile will be complex and difficult to determine without combining a transient study with a six degree of freedom analysis.

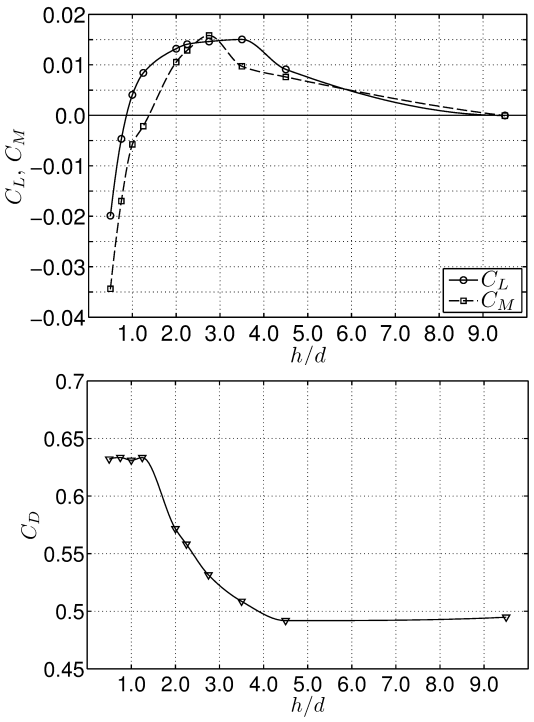

Figure 6: Coefficient of lift and moment (based on planform area) and drag (based on frontal area) as functions of ground separation distance h/d.

Early inference can be made about the general features of transonic ground effect aerodynamics by considering the presented force, moment, pressure and velocity data. Firstly, in all the computational simulations a band of supersonic flow exists around the entire circumference of the projectile. As communication in supersonic flow can only occur downstream, the properties beyond the supersonic band are incapable of influencing the properties of the flow in front of the band, except through the (subsonic) boundary layer on the projectile itself. This means the stand-off distance of the bow shock is unlikely to be influenced by changes seen in the wake behaviour. The subsonic region immediately behind the strong solution portion of the bow shock, however, extends to nearly half the projectile length. The projectile's geometrical features such as width and lengthwise gradient changes, and how these features combine with the ground plane to reduce the flow area underneath the projectile, will most certainly be felt by the bow shock. It is thus the equilibrium reached between the flow around the forward half of the projectile and the bow shock which primarily dictates the resulting pitching moment, lift and drag forces on the projectile.

Conclusions

A range of ground separation distances h/d were investigated to establish how the ground influences the aerodynamic forces and moments on a transonic projectile. Three different conditions were identified in this study. Condition A ($0.5 < h/d < 0.85$) is characterised by a force acting towards the ground plane with a nose up pitching moment. The greatest magnitude in lift was measured to be 10% of the projectile's drag (noting the different reference areas used for C_L and C_D in figure 6). Condition B ($0.85 < h/d < 1.5$) is characterised by a lift force acting away from the ground plane with a very small nose up pitching moment. Condition C ($h/d > 1.5$) is characterised by a gradual increase in the coefficient of lift with a nose down pitching moment that also increases very gradually, until both peak at about $h/d = 2.75 - 3.0$ and then asymptote to zero with further increase in h/d. The bow shock stand-off distance s/d was also demonstrated to be strongly correlated to the ground clearance. The stand-off distance grows rapidly with a reduction in ground clearance. In summary, the results of this study support the vertical force and increased bow shock stand-off distance seen in previous wind-tunnel experiments. Further CFD analysis is required to estimate the time taken for the flow field to reach equilibrium in order to assist with changes to the live fire experimental set-up.

References

[1] Doig, G., Barber, J., Leonardi, E., Neely, A.J., Kleine, H., Aerodynamics of a supersonic projectile in close proximity to a solid surface, *AIAA Journal* **48**(12), 2010, 2916–2930.

[2] Halloran, M., O'Meara, S., Wing in Ground Effect Craft Review, Defence Science and Technology Organisation, Melbourne, 2000.

[3] Kleine, H., Hiraki, K., Oakes, B., Young, J., Kusano, H., Inatani, Y., Projectiles in transonic ground effect, *Proc. 29th Int. Congr. High-Speed Imaging & Photonics*, Morioka, Japan, September 20-24, 2010.

[4] Massey, K.C., Silton, S.I., Combining experimental data, computational fluid dynamics and six-degree of freedom simulation to develop a guidance actuator for supersonic flow, *Journal of Aerospace Engineering* **233**(G), 341–355, 2009.

[5] Morgan, K., Hassan, O., Weatherill, N.P., Why didn't the supersonic car fly? *Mathematics Today, Bulletin of the Institute of Mathematics and its Applications* **35** (4), 110–114, 1999.

[6] Purdon, J., Mudford, N.R., Kleine, H., Supersonic projectiles in the vicinity of solid obstacles, *Proc. 27th Int. Congr. High-Speed Photography & Photonics*, Xian, China, SPIE Vol. 6279, 2006.